Single pulse laser-induced breakdown spectroscopy of bulk aqueous solutions at oceanic pressures: interrelationship of gate delay and pulse energy

Anna P. M. Michel[1,2,3,*] and Alan D. Chave[1]

[1]Department of Applied Ocean Physics and Engineering, Woods Hole Oceanographic Institution, Mail Stop 7, 266 Woods Hole Road, Woods Hole, Massachusetts 02543, USA

[2]Department of Mechanical Engineering, Massachusetts Institute of Technology, 77 Massachusetts Avenue, Cambridge, Masachusetts 02139, USA

[3]Currently at the Center for Mid-InfraRed Technologies for Health and the Environment, Princeton Institute for the Science and Technology of Materials, Princeton University, 70 Prospect Avenue, Princeton, New Jersey 08540, USA

*Corresponding author: apmichel@princeton.edu

Received 31 March 2008; revised 2 August 2008; accepted 12 August 2008; posted 12 August 2008 (Doc. ID 94499); published 19 September 2008

The ability of oceanographers to make sustained measurements of ocean processes is limited by the number of available sensors for long-term *in situ* analysis. In recent years, laser-induced breakdown spectroscopy (LIBS) has been identified as a viable technique to develop into an oceanic chemical sensor. We performed single pulse laser-induced breakdown spectroscopy of high pressure bulk aqueous solutions to detect three analytes (sodium, manganese, and calcium) that are of key importance in hydrothermal vent fluids, an ocean environment that would greatly benefit from the development of an oceanic LIBS sensor. The interrelationship of the key experimental parameters, pulse energy and gate delay, for a range of pressures up to 2.76×10^7 Pa, is studied. A minimal effect of pressure on the peak intensity is observed. A short gate delay (less than 200 ns) must be used at all pressures. The ability to use a relatively low laser pulse energy (less than ≈60 mJ) for detection of analytes at high pressure is also established. Na, Mn, and Ca are detectable at pressures up to 2.76×10^7 Pa at 50, 500, and 50 ppm, respectively, using an Echelle spectrometer.

OCIS codes: 140.3440, 140.0140, 010.4450, 300.0300, 300.6365.

1. Introduction

New chemical sensors are needed for oceanic process studies and are of critical importance as oceanography shifts to a new operational mode using permanent ocean observatories. New sensors take a significant time to develop and transform from benchtop laboratory prototypes to ocean-going systems. The development phase first requires validation that an analytical technique will work under *in situ* conditions.

Laser-induced breakdown spectroscopy (LIBS) is a type of atomic emission spectroscopy that has been identified as a viable technique for use as a field-going sensor for geochemical and environmental sensing [1]. For example, a new mobile instrument has been developed for evaluating polluted soils [2,3]. Palanco *et al.* proposed a field deployable LIBS system for standoff measurements at hundreds of meters range [4]. Several groups have investigated LIBS for space exploration [5–10]. Courrèges-Lacoste *et al.* [7] are developing a combined Raman/LIBS instrument for investigating past and present life on Mars. Arp *et al.* [6] have investigated the use of LIBS in the high temperature (>700 K), high pressure (of the order of 9×10^6 Pa) environment of Venus. Another proposed *in situ* application of LIBS is its development into an oceanic chemical sensor [11–13].

0003-6935/08/31G122-09$15.00/0

One oceanic environment that would benefit greatly from the development of such a sensor is the hydrothermal vents that occur at mid-ocean ridges where seawater circulates through the permeable ocean crust. As seawater moves through high temperature rock, the fluid interacts with it, inducing major chemical changes to both the rock and the fluid. At vent orifices, exit temperatures reach 200–405 °C at ambient pressures from 8.1×10^6 to 3.6×10^7 Pa, corresponding to ocean depths of 800–3600 m [14]. Conventional analytical measurement of the fluids is difficult due to the corrosive nature of the vent environment and irreversible changes in composition that occur when they are removed to the surface.

Three key elements in vent fluid studies are sodium, calcium, and manganese. Sodium is the most abundant cation in vent fluids and helps in understanding phase separation processes [15]. Manganese exists as a trace metal in seawater but is leached from the host rock so that it is present at higher concentrations in vent fluids [15]. When measured simultaneously with Fe, Mn can be used as an indication of subsurface mineralization, as Fe precipitates out while Mn stays in solution. Calcium is the second most abundant cation in vent fluids and is typically enriched when compared to seawater [16]. Ca is released into vent fluids when sodium is taken up during albitization reactions with the host rock. In vent fluids, concentrations range from approximately 250 to 23,163 ppm for Na, 0.6 to 399 ppm for Mn, and 0 to 4477 ppm for Ca [14]. In seawater, concentrations are approximately 10,933 ppm Na, <0.001 ppm Mn, and 419 ppm Ca [14].

There is limited prior work on the study of dissolved analytes within bulk aqueous solutions [11–13,17–20] due to inherent difficulties of detection. The plasma formed in bulk liquid displays reduced light intensity and a reduction in emission lifetime due to quenching [17,18,21,22]. In addition, spectral lines may be broadened through the Stark effect [17]. Furthermore, "moving breakdown" occurs that randomly changes the distance between the plasma and the collection optics, a phenomenon that is not important for plasma formation on solids. The plasma expands along the beam path of the laser, resulting in an elongated plasma that cavitates cylindrically [23]. For many aqueous applications, these issues can be avoided by analysis on a liquid surface, jet, or film; however, for the development of an *in situ* oceanic system, it is necessary to work directly within bulk liquids.

Although we have previously reported on the successful use of LIBS for detection of bulk aqueous analytes at high pressure (up to 2.76×10^7 Pa) [11–13], the development of LIBS into an oceanic chemical sensor requires optimization of the experimental system to maximize the signal-to-background ratio (SBR) of the spectra and improve the limit of detection. In this work, a comprehensive study of the effect of the two key parameters for single pulse LIBS on SBR was completed. Peak intensities were measured to determine optimal conditions for the detection of Na, Ca, and Mn at high pressure. Subsequently, calibration curves were constructed to estimate the limits of detection using an Echelle spectrometer.

2. Experimental

The laboratory setup for simulating a LIBS sensor in the deep ocean is depicted in Fig. 1. Plasma formation is induced with a Big Sky CFR-200 Nd:YAG laser operated at 1064 nm with a 5 Hz repetition rate. The laser is equipped with a motorized variable attenuator, serially controlled by a computer, enabling the laser pulse energy (E) to be varied from 0 to 200 mJ in increments of approximately 1 mJ. Plasma emission is collected with an Echelle spectrometer (LLA Echelle ESA 3000) capable of detecting wavelengths between 200 and 780 nm with a spectral resolution of 10–50 pm. Timing control of the laser and turn-on of the spectrometer are managed by a timing box (Berkeley Nucleonics Corporation Model 565). The single pulse LIBS timing parameters are gate delay (t_d, the time between the laser pulse and turn-on of the spectrometer) and gate width (t_b, the integration time of the spectrometer).

An 8.89 cm × 8.89 cm × 8.89 cm titanium sample chamber that holds 27 ml of liquid is connected to a high pressure metering pump (Eldex Model A-30-S) that is used to pressurize samples to 4.1×10^7 Pa. The sample chamber is equipped with a sapphire window (Meller Optics, 2.54 cm

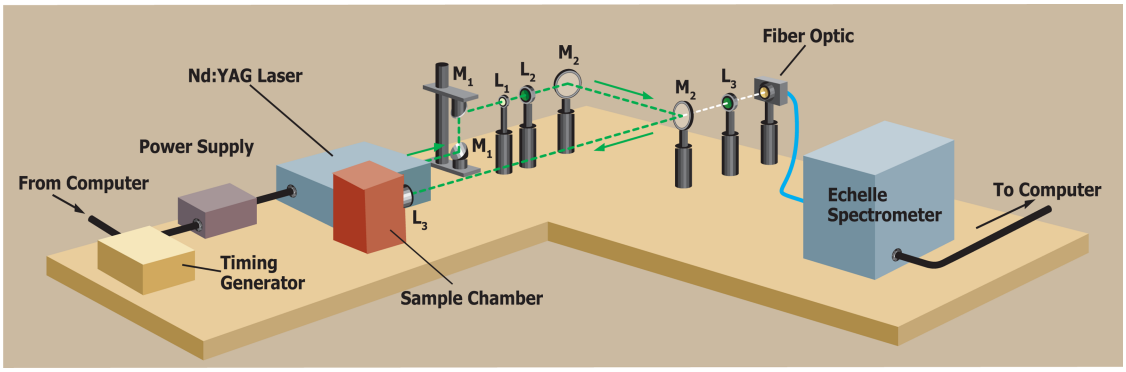

Fig. 1. (Color online) LIBS laboratory setup. $M_1 = 25$ mm diameter, 1064 nm Nd:YAG mirror; $L_1 = 12$ mm × −12 mm lens; $L_2 = 25$ mm × 50 mm lens; $M_2 = 50$ mm diameter, 1064 nm Nd:YAG mirror; $L_3 = 25$ mm × 35 mm lens.

diameter × 0.64 cm thickness, antireflection coated at 532 nm/1064 nm, custom part) that enables laser pulses to enter the sample chamber. A series of antireflection-coated optics are used to focus the laser beam into the sample chamber, with the final focusing lens fitted into the sample chamber. An additional lens is used to focus the plasma light onto an optical fiber and deliver it to the Echelle spectrometer. The plasma light is collected collinear to the incoming laser beam. This optical geometry was selected because it is the practical configuration for an ocean-going LIBS system. Data were collected using ESAWIN software. Laser energy is measured using a laser energy sensor (Coherent J25LP-MB) combined with an energy meter (Coherent FieldMaxII-Top).

To determine optimal conditions for the detection of the three analytes, spectral intensities were measured over a range of LIBS system parameters. For Na and Mn, detailed studies were conducted at five pressures (1×10^5, 6.89×10^6, 1.38×10^7, 2.07×10^7, and 2.76×10^7 Pa, which correspond to ocean depths of approximately 0, 680, 1361, 2041, and 2722 m, respectively). For Ca, the studies were conducted at three pressures (1×10^5, 1.38×10^7, and 2.76×10^7 Pa). The parameters t_d and E were systematically varied to determine their effect on both plasma intensity and SBR. Five spectra were taken for each parameter pair, each composed of 100 accumulated shots. E ranged from 10 to 170 mJ in 10 mJ increments. Laser beam waist width d_{σ_o} can be estimated for the apparatus from

$$d_{\sigma_o} = \frac{4f\lambda M^2}{\pi D}, \tag{1}$$

where f is the focal length of the focusing lens (35 mm), λ is the laser wavelength (1064 nm), M^2 is the beam propagation ratio, which is typically 2–10 for Nd:YAG lasers (we therefore choose a value of 6), and D is the diameter of the illuminated aperture of the focusing lens (≈25 mm) [24]. The beam waist width for the system is approximately 0.07 mm. The average irradiance (I_f) at the beam waist is

$$I_f = \frac{\pi E D^2}{4\tau_L f^2 \lambda^2 M^4}, \tag{2}$$

where $\tau_L (= 7.5\,\text{ns})$ is the pulse duration at the full peak width at half of the maximum intensity (FWHM) [24]. E was varied between 10 and 170 mJ, resulting in variation of irradiance at the beam waist from ≈1.31×10^{12} to 2.23×10^{13} W/cm^2. The t_d used was 50, 75, 100, 125, 150, 200, 300, and 500 ns. Each combination of E and t_d was tested, resulting in 136 different conditions for the optimization studies.

The signal-to-background ratio is defined by

$$\text{SBR} = 20\log_{10}\frac{\text{amplitude}_{\text{peak}}}{\text{amplitude}_{\text{background}}}, \tag{3}$$

where the amplitude of the background is the spectral average over a region where no peaks are expected. The background was calculated for Na by using the spectral region from 200 to 500 nm and for Mn and Ca by using the spectral region from 430 to 530 nm.

All raw spectra were processed using extreme value distribution statistics previously described by Michel and Chave [25]. Data from nine wavelengths were grouped for processing. Where shown, error bars represent the double sided 95% confidence limits [25]. Calibration curves were made for Na, Ca, and Mn, with 10 spectra being taken at each concentration, each composed of 100 accumulated shots. The experimental conditions used for the calibration curves are detailed in Table 1. For each analyte, a linear least squares fit of the concentration data was computed in addition to 95% confidence limits on the coefficients. For all the experiments, t_b was held constant at 200 ns. In addition, the amplification of the Echelle spectrometer was set to its maximum value of 4000. Solutions were made from NaCl, $MnSO_4 \cdot H_2O$, and $CaCl_2 \cdot 2H_2O$ dissolved in DI water for the Na, Mn, and Ca studies, respectively. All concentrations are given in parts per million (ppm, wt./vol.).

3. Results and Discussion

A. Sodium

The interrelationship of t_d and E for sodium was studied at a concentration of 100 ppm. The intensity of the 588.995 nm Na (I) peak was measured. As pressure rises, an increase in signal intensity is observed, with the maximum peak intensity present at 2.76×10^7 Pa (data not shown). The greatest peak intensity exists at the shortest t_d. As t_d increases, peak intensity decreases, independent of both E and ambient pressure. Overall, there appears to be little effect of E on intensity. Examination of the SBR provides important information for selecting optimal parameters. Figure 2 details the interrelationship of t_d, E, and SBR. A smaller t_d tends to exhibit a higher SBR due to a stronger signal. Furthermore, Fig. 2 suggests that a lower E consistently provides a higher SBR. As pressure increases, SBR tends to increase. The data suggest that the highest SBR exists when a low E (20–60 mJ) and a relatively small t_d (50–150 ns) are used. As first reported in Michel *et al.* [11], this suggests that an optimal range of E exists that tends to be relatively low.

For the best SBR, an E of 40 mJ and a t_d of 50 ns were identified for detection of Na (I) over a range of pressures, and spectra under this condition are

Table 1. Calibration Curve Conditions

Analyte	Concentrations Tested (ppm)	E (mJ)	t_d (ns)
Na	0.05, 0.1, 0.5, 1, 5, 10, 50, 100, 500, 1000	40	50
Mn	1, 5, 10, 50, 100, 500, 1000	30	50
Ca	1, 5, 10, 50, 100, 500, 1000	30	50

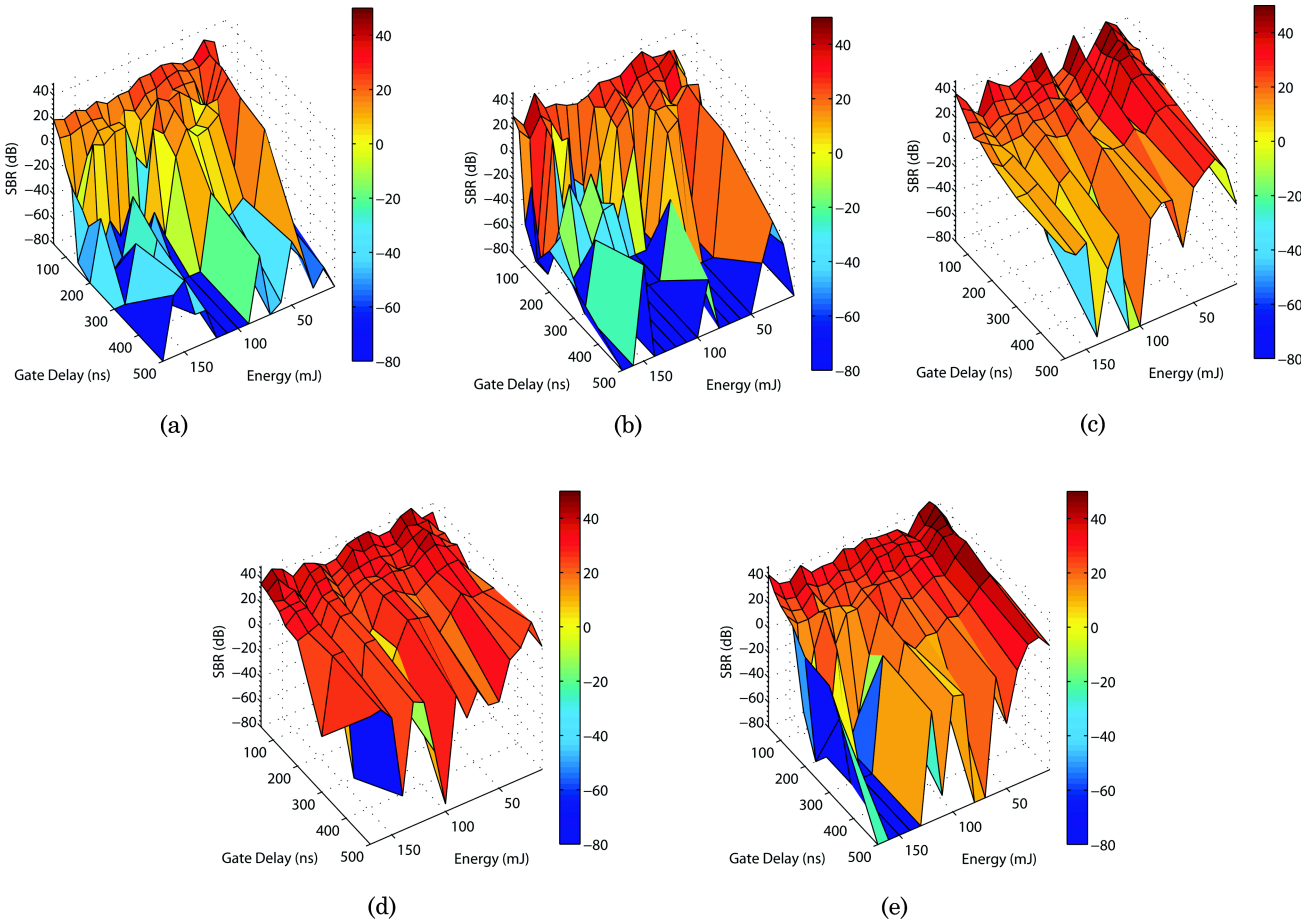

Fig. 2. Interrelationship of pressure, gate delay, energy, and SBR for Na (588.995 nm) (a) 1×10^5 Pa, (b) 6.89×10^6 Pa, (c) 1.38×10^7 Pa, (d) 2.07×10^7 Pa, (e) 2.76×10^7 Pa.

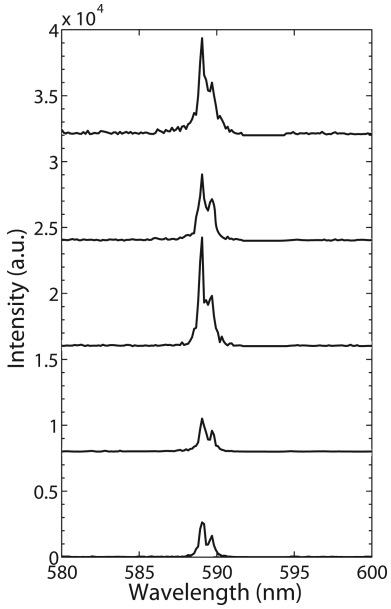

Fig. 3. Spectra of Na (588.995 nm and 589.6 nm) taken with a pulse energy of 40 mJ and a gate delay of 50 ns. From bottom to top, the spectra were taken at 1×10^5 Pa, 6.89×10^6 Pa, 1.38×10^7 Pa, 2.07×10^7, and 2.76×10^7 Pa. For clarity, the spectra have been offset from each other by 8000 a.u.

plotted in Fig. 3. Calibration curves for Na (I) were constructed to determine the limit of detection (Fig. 4). These suggest that Na (I) can be detected at a concentration of approximately 50 ppm using the present apparatus with no pressure effect on the detection limit. Spectra of the Na (I) calibration data are shown in Fig. 5.

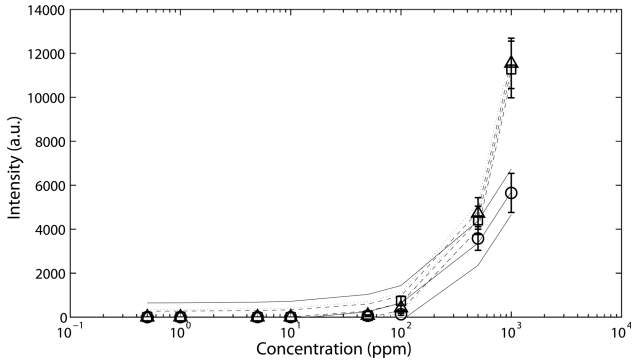

Fig. 4. Calibration curves calculated by a linear least squares fit of the concentration data and their 95% confidence limits on the coefficients for the 588.995 nm sodium peak. ○, solid line = 1×10^5 Pa; □, dashed line = 1.38×10^7 Pa; △, dotted line = 2.76×10^7 Pa.

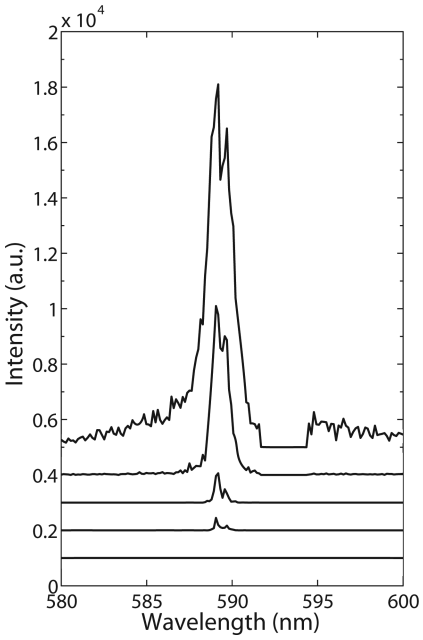

Fig. 5. Spectra of sodium (588.995 nm and 589.6 nm) at 2.76×10^7 Pa made over a range of NaCl concentrations. The concentrations from bottom to top are 10 ppm, 50 ppm, 100 ppm, 500 ppm, and 1000 ppm. For clarity, the spectra have been offset from each other by 1000 a.u.

B. Manganese

The effect of E and t_d on spectra for manganese was studied using a concentration of 1000 ppm Mn (I) over a range of pressures. Although a Mn (I) triplet exists at 403 nm, peak broadening in liquids makes its individual elements unresolvable, and therefore we report on a single 403 nm peak. The interrelationship of pressure, t_d, E, and intensity was examined, and it was found that as pressure increases, peak intensity also rises (data not shown). A similar finding was reported by Michel *et al.* for a single tested condition (single E and t_d) [11]. Irrespective of t_d and E, the peak intensity of Mn (I) was found to increase with pressure. When the corresponding SBRs are examined (Fig. 6), SBR is shown to be smallest at the lowest pressure (1×10^5 Pa). Again, the need for a short t_d and the ability to use a low E are evident.

From the optimization studies, an E of 30 mJ with a t_d of 50 ns was selected as a condition that would allow for the detection of Mn (I) over a broad range of pressures. The selected condition is plotted for five pressures in Fig. 7. To determine the limit of detection of Mn (I), a calibration curve was constructed using an E of 30 mJ and a t_d of 50 ns (Fig. 8). Figure 9 shows spectra made under

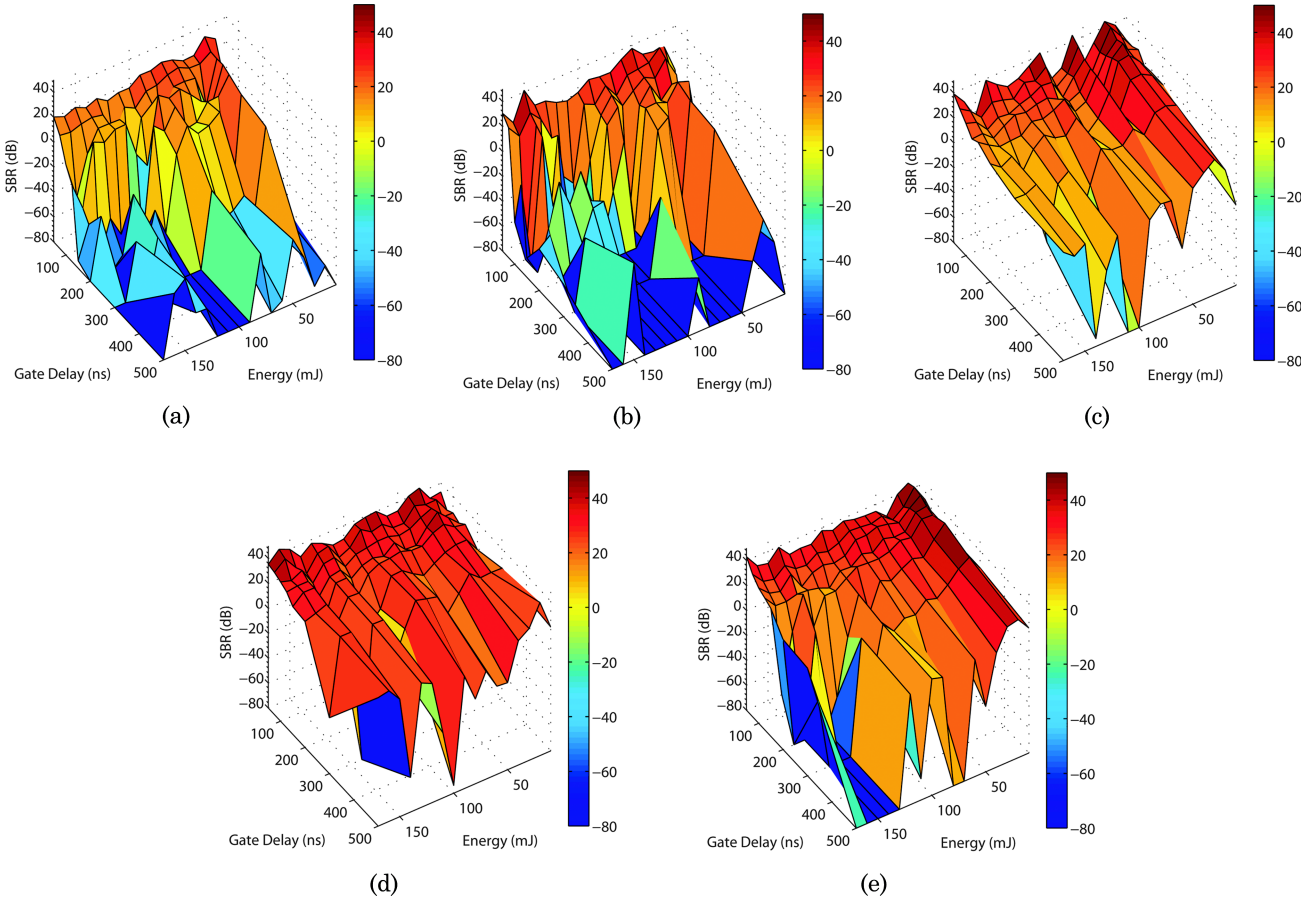

Fig. 6. Interrelationship of pressure, t_d, E, and SBR for Mn (403.076 nm) (a) 1×10^5 Pa, (b) 6.89×10^6 Pa, (c) 1.38×10^7 Pa, (d) 2.07×10^7 Pa, (e) 2.76×10^7 Pa.

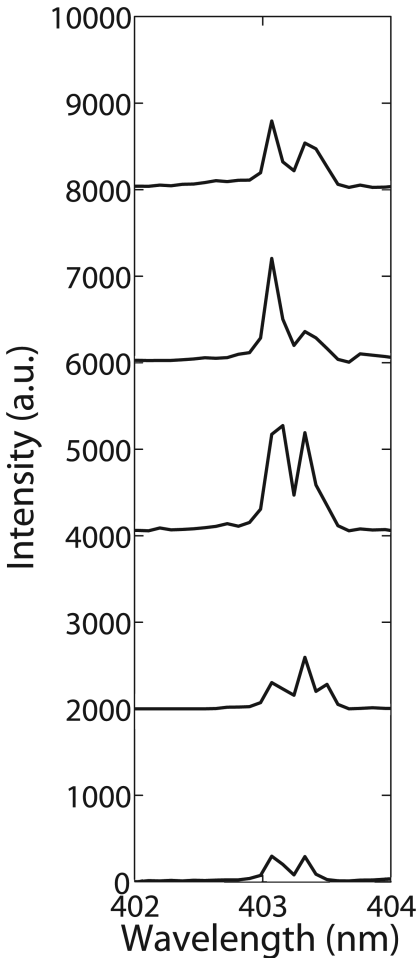

Fig. 7. Manganese (403 nm peak) spectra using a 30 mJ energy pulse and a gate delay of 50 ns. The spectra from bottom to top are at 1×10^5 Pa, 6.89×10^6 Pa, 1.38×10^7 Pa, 2.07×10^7 Pa, 2.76×10^7 Pa. For clarity, the spectra have been offset from each other by 2000 a.u.

these conditions at 2.76×10^7 Pa over a range of concentrations. The limit of detection was found to be 500 ppm for the present apparatus, which is still higher than the concentration found in vent fluids. Again, very little pressure effect on the detection of Mn was found.

C. Calcium

Two calcium peaks, Ca (II) 393 nm (ionic) and Ca (I) 422 nm (atomic), were studied. The interrelationship of the measurement parameters of Ca was determined and is shown in Figs. 10 and 11. The importance of a short t_d is evident. E appears to have relatively little influence on SBR at most pressures, which is unlike the effect seen for Na, possibly due to the higher ionization energy of Ca. Although three calcium peaks are actually detectable (393, 396, and 422 nm), the 422 nm peak is the strongest, and therefore the selection of optimal conditions was based on this peak. An E of 30 mJ with a t_d of 50 ns was selected for detection of Ca, and spectra illustrating this are shown in Fig. 12.

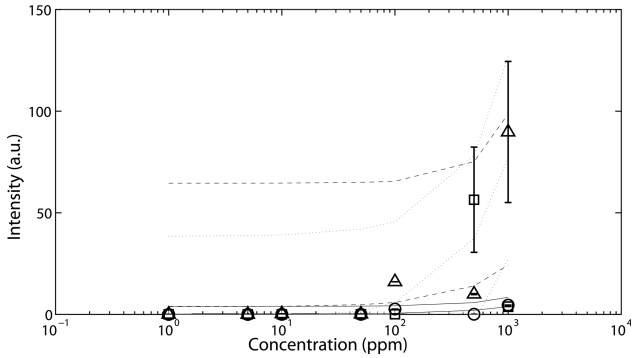

Fig. 8. Calibration curves and their 95% confidence limits for the 403 nm manganese peak. ○, solid line = 1×10^5 Pa; □, dashed line = 1.38×10^7 Pa; △, dotted line = 2.76×10^7 Pa.

Calcium calibration curves were constructed and are shown in Fig. 13 for both the 393 and the 422 nm peaks. These suggest that the limit of detection for Ca is 50 ppm using the present apparatus for the three pressures evaluated. Spectra for selected concentrations are illustrated in Fig. 14.

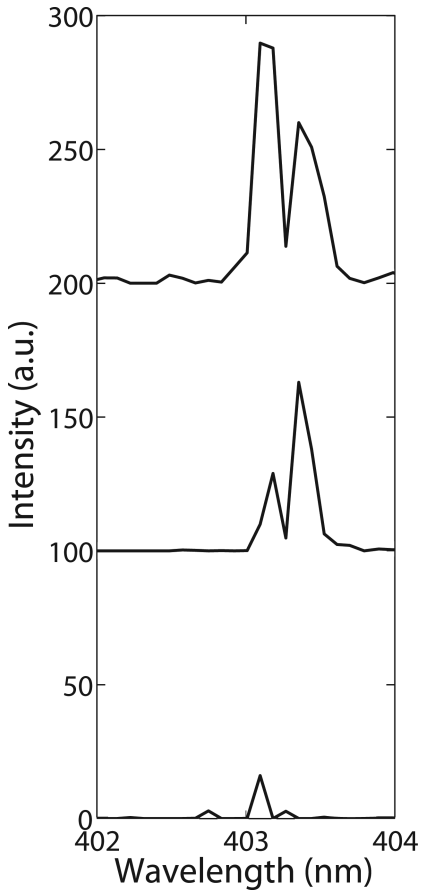

Fig. 9. Spectra of manganese at 2.76×10^7 Pa made over a range of concentrations from bottom to top, the concentrations are 100 ppm, 500 ppm, and 1000 ppm. For clarity, the spectra have been offset from each other by 100 a.u.

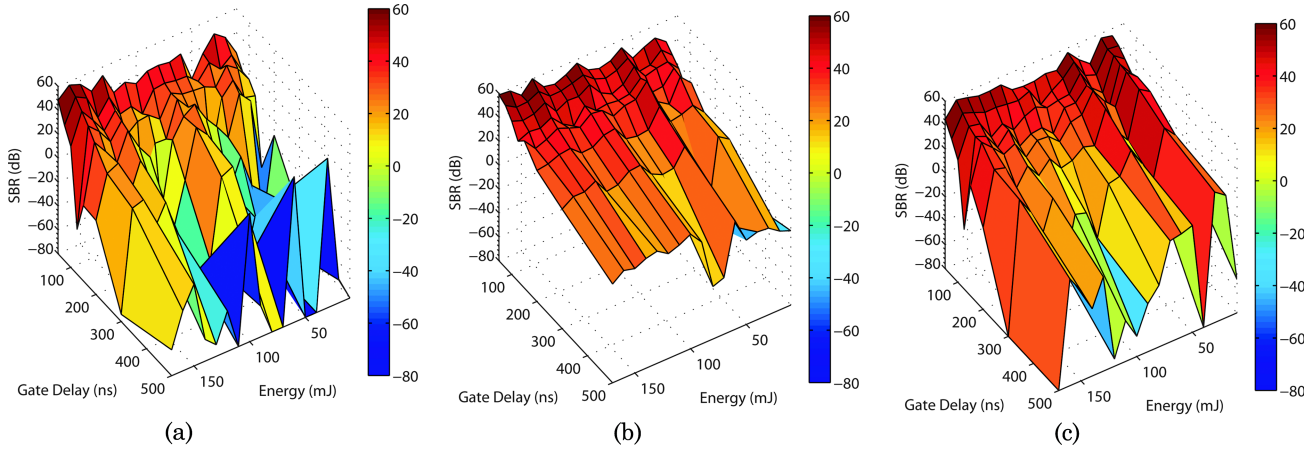

Fig. 10. Interrelationship of pressure, t_d, E, and signal-to-background for Ca (393 nm) (a) 1×10^5 Pa, (b) 1.38×10^7 Pa, (c) 2.76×10^7 Pa.

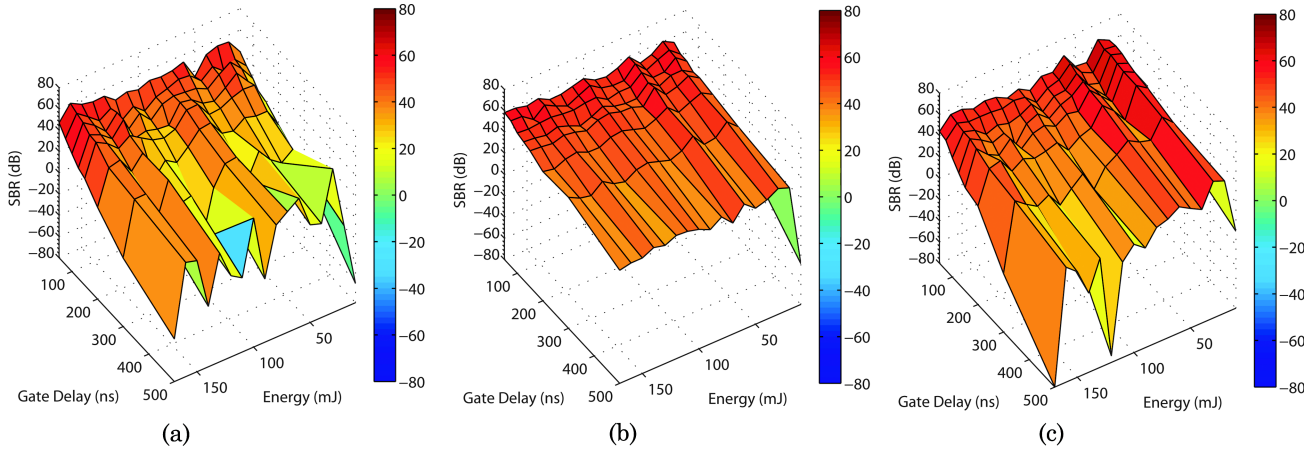

Fig. 11. Interrelationship of pressure, t_d, E, and SBR for Ca (422 nm) (a) 1×10^5 Pa (b) 1.38×10^7 Pa (c) 2.76×10^7 Pa.

4. Conclusions

Sodium, manganese, and calcium are all detectable in high pressure, bulk aqueous solutions using single pulse LIBS with little effect of pressure on the spectra. This comprehensive study of the interrelationship of t_d and E for selecting the optimal condition for detection of these analytes has shown that, irrespective of E selected, the t_d should be very short (less than 200 ns). The need for a short t_d is independent of pressure. The short t_d is a result of the reduced lifetime of plasma emission in bulk solutions due to quenching of the plasma by the liquid. This study has also shown that a low E (less than ≈60 mJ) is sufficient. Using a higher E may cause greater plasma shielding and moving breakdown. Moving breakdown can result in the plasma becoming elongated and the breakdown occurring away from the collection focal point. Thus, the effects of plasma shielding and moving breakdown can be detrimental for plasma emission collection.

Calibration curves were constructed to determine limits of detection using the current system setup, and further work is needed to look at reproducibility of the actual curves. Laboratory data show that Na, Mn, and Ca can be detected at 50, 500, and 50 ppm,

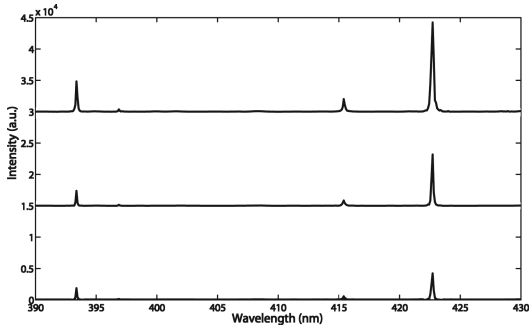

Fig. 12. Calcium spectra using 30 mJ and a 50 ns gate delay. Calcium peaks (393 nm, 396 nm, and 422 nm). Spectra from bottom to top: 1×10^5 Pa, 1.38×10^7 Pa, and 2.76×10^7 Pa. For clarity, the spectra have been offset from each other by 15,000 a.u.

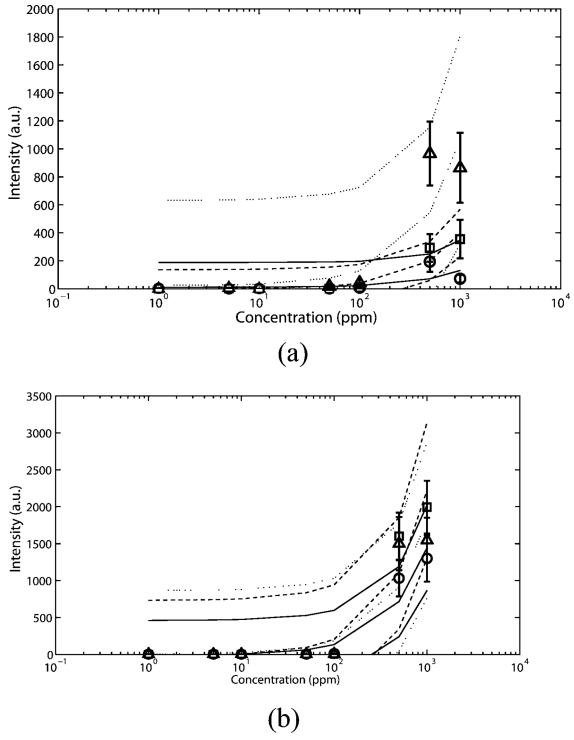

Fig. 13. Calibration curves calculated by a linear least squares fit of the concentration data and their 95% confidence limits on the coefficients for the (a) 393 nm and (b) 422 nm calcium peaks. ○, solid line = 1×10^5 Pa; □, dashed line = 1.38×10^7 Pa; △, dotted line = 2.76×10^7 Pa.

respectively. The calibration curves also demonstrate a minimal effect of pressure on spectra. However, the limits of detection were higher than expected. With the current LIBS setup, the detection limits of Na and Ca are below the levels found in vent fluids. However, Mn would not be detectable. This can be attributed to the low light throughput of the $f/10$ Echelle system. To significantly improve the light throughput, it would be advisable to use a spectrometer with a smaller f number. For example, using a spectrometer with an f number of 2 could improve the throughput by a factor of approximately 25 and therefore improve the ability to detect Na, Mn, and Ca in high pressure aqueous environments. Using a photomultiplier tube as the detector, Cremers *et al.* [17] showed substantially improved detection limits in bulk liquids at atmospheric pressure for Na I (589.00 nm) of 0.014 ppm and Ca II (393.37 nm) of 0.8 ppm. Therefore, additional work is necessary to optimize the light collection by changing the system components.

We acknowledge the National Science Foundation (NSF) for support of this research under grant OCE-0527927. Additional support was received from the Deep Ocean Exploration Institute and the Ocean Ventures Fund of the Woods Hole Oceanographic Institution.

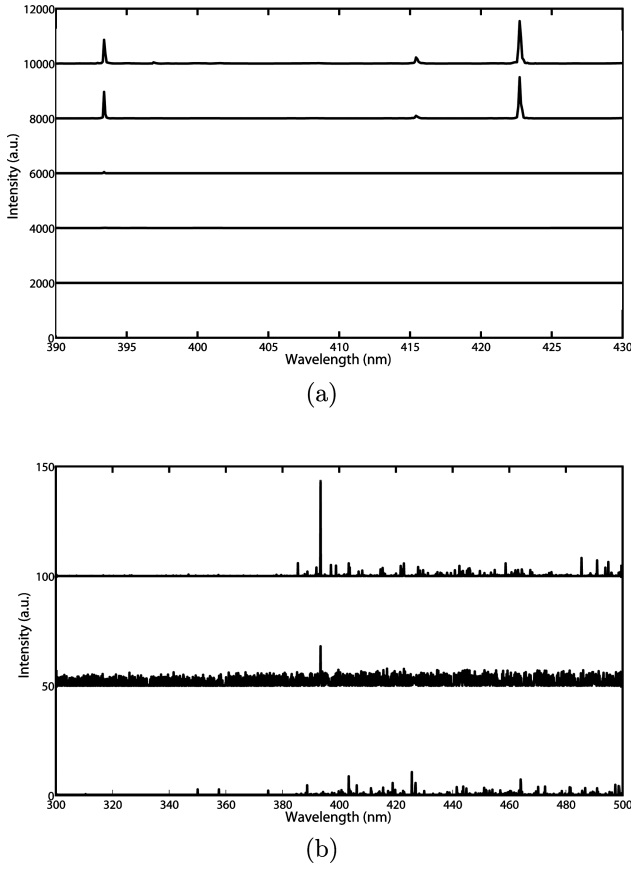

Fig. 14. Calcium spectra at 2.76×10^7 Pa with peaks present at 393 nm, 396 nm, and 422 nm. (a) Spectra from bottom to top are 10 ppm, 50 ppm, 100 ppm, 500 ppm, 1000 ppm, respectively. For clarity, the spectra have been offset from each other by 2000 a.u. (b) Spectra from bottom to top are 10 ppm, 50 ppm, and 100 ppm, respectively. For clarity, the spectra have been offset from each other by 50 a.u.

References

1. R. S. Harmon, F. C. DeLucia, C. E. McManus, N. J. McMillan, T. F. Jenkins, M. E. Walsh, and A. Miziolek, "Laser-induced breakdown spectroscopy—an emerging chemical sensor technology for real-time field-portable, geochemical, mineralogical, and environmental applications," Appl. Geochem. **21**, 730–747 (2006).
2. A. Bertolini, G. Carelli, F. Francesconi, M. Francesconi, L. Marchesini, P. Marsili, F. Sorrentino, G. Cristoforetti, S. Legnaioli, V. Palleschi, L. Pardini, and A. Salvetti, "Modi: a new mobile instrument for in situ double-pulse LIBS analysis," Anal. Bioanal. Chem. **385**, 240–247 (2006).
3. M. Corsi, G. Cristoforetti, M. Hidalgo, S. Legnaioli, V. Palleschi, A. Salvetti, E. Tognoni, and C. Vallebona, "Double pulse, calibration-free laser-induced breakdown spectroscopy: a new technique for in situ standard-less analysis of polluted soils," Appl. Geochem. **21**, 748–755 (2006).
4. S. Palanco, C. Lopez-Moreno, and J. J. Laserna, "Design, construction and assessment of a field-deployable laser-induced breakdown spectrometer for remote elemental sensing," Spectrochim. Acta Part B **61**, 88–95 (2006).
5. Z. A. Arp, D. A. Cremers, R. C. Wiens, D. M. Wayne, B. Sall, and S. Maurice, "Analysis of water ice and water ice/soil mixtures using laser-induced breakdown spectroscopy: appli-

cation to Mars polar exploration," Appl. Spectrosc. **58**, 897–909 (2004).
6. Z. A. Arp, D. A. Cremers, R. D. Harris, D. M. Oschwald, G. R. Parker, Jr., and D. M. Wayne, "Feasibility of generating a useful laser-induced breakdown spectroscopy plasma on rocks at high pressure: preliminary study for a Venus mission," Spectrochim. Acta Part B **59**, 987–999 (2004).
7. G. B. Courrèges-Lacoste, B. Ahlers, and F. R. Pérez, "Combined Raman spectrometer/laser-induced breakdown spectrometer for the next ESA mission to Mars," Spectrochim. Acta Part A **68**, 1023–1028 (2007).
8. R. Brennetot, J. L. Lacour, E. Vors, A. Rivoallan, D. Vailhen, and S. Maurice, "Mars analysis by laser-induced breakdown spectroscopy (MALIS): Influence of Mars atmosphere on plasma emission and study of factors influencing plasma emission with the use of Doehlert designs," Appl. Spectrosc. **57**, 744–752 (2003).
9. A. Knight, N. Scherbarth, D. Cremers, and M. Ferris, "Characterization of laser-induced breakdown spectroscopy (LIBS) for application to space exploration," Appl. Spectrosc. **54**, 331–340 (2000).
10. B. Sallé, J.-L. Lacour, P. Mauchien, P. Fichet, S. Maurice, and G. Manhes, "Comparative study of different methodologies for quantitative rock analysis by laser-induced breakdown spectroscopy in a simulated Martian atmosphere," Spectrochim. Acta Part B **61**, 301–313 (2006).
11. A. P. M. Michel, M. Lawrence-Snyder, S. M. Angel, and A. D. Chave, "Laser-induced breakdown spectroscopy of bulk aqueous solutions at oceanic pressures: evaluation of key measurement parameters," Appl. Opt. **46**, 2507–2515 (2007).
12. M. Lawrence-Snyder, J. Scaffidi, S. M. Angel, A. P. M. Michel, and A. D. Chave, "Sequential-pulse laser-induced breakdown spectroscopy of high-pressure bulk aqueous solutions," Appl. Spectrosc. **61**, 171–176 (2007).
13. M. Lawrence-Snyder, J. Scaffidi, S. M. Angel, A. P. M. Michel, and A. D. Chave, "Laser-induced breakdown spectroscopy of high-pressure bulk aqueous solutions," Appl. Spectrosc. **60**, 786–790 (2006).
14. C. R. German and K. L. Von Damm, "Hydrothermal processes," in *Treatise on Geochemistry*, H. Elderfield, H. D. Holland, and K. K. Turekian, eds. (Elsevier, 2003), Vol. 6, pp. 181–222.
15. K. L. Von Damm, "Controls on the chemistry and temporal variability of seafloor hydrothermal fluids," in *Seafloor Hydrothermal Systems: Physical, Chemical, Biological, and Geological Interactions*, Geophysical Monograph No. 91, S. Humphris, L. Mullineaux, R. Zierenberg, and R. Thomson, eds. (American Geophysical Union, 1995), pp. 222–249.
16. K. L. Von Damm, "Chemistry of hydrothermal vent fluids from 9°–10° N, East Pacific Rise: 'Time zero,' the immediate posteruptive period," J. Geophys. Res. **105**, 11203–11222 (2000).
17. D. A. Cremers, L. J. Radziemski, and T. R. Loree, "Spectrochemical analysis of liquids using the laser spark," Appl. Spectrosc. **38**, 721–729 (1984).
18. R. Knopp, F. J. Scherbaum, and J. I. Kim, "Laser induced breakdown spectroscopy (LIBS) as an analytical tool for the detection of metal ions in aqueous solutions," Anal. Bioanal. Chem. **355**, 16–20 (1996).
19. W. Pearman, J. Scaffidi, and S. M. Angel, "Dual-pulse laser-induced breakdown spectroscopy in bulk aqueous solution with an orthogonal beam geometry," Appl. Opt. **42**, 6085–6093 (2003).
20. A. De Giacomo, M. DellAglio, F. Colao, R. Fantoni, and V. Lazic, "Double-pulse LIBS in bulk water and on submerged bronze samples," Appl. Surf. Sci. **247**, 157–162 (2005).
21. A. E. Pichahchy, D. A. Cremers, and M. J. Ferris, "Elemental analysis of metals under water using laser-induced breakdown spectroscopy," Spectrochim. Acta Part B **52**, 25–39 (1997).
22. C. Haisch, J. Liermann, U. Panne, and R. Niessner, "Characterization of colloidal particles by laser-induced plasma spectroscopy (LIPS)," Anal. Chim. Acta **346**, 23–25 (1997).
23. P. K. Kennedy, D. X. Hammer, and B. A. Rockwell, "Laser-induced breakdown in aqueous media," Prog. Quantum Electron. **21**, 155–248 (1997).
24. R. Noll, "Terms and notations for laser-induced breakdown spectroscopy," Anal. Bioanal. Chem. **385**, 214–218 (2006).
25. A. P. M. Michel and A. D. Chave, "Analysis of laser-induced breakdown spectroscopy spectra: the case for extreme value statistics," Spectrochim. Acta Part B **62**, 1370–1378 (2007).